Full spectrum millimeter-wave modulation in thin-film $LiNbO_3$

Andrew J. Mercante
University of Delaware
Newark, Delaware United States
ajmerc@udel.edu

Shouyuan Shi
University of Delaware
Newark, Delaware United States
sshi@udel.edu

Peng Yao
Phase Sensitive Incorporated
Newark, Delaware United States
yao@phasesensitiveinc.com

Dennis W. Prather
University of Delaware
Newark, Delaware United States
dprather@udel.edu

***Abstract*— We present a crystal ion sliced (CIS) $LiNbO_3$ phase modulator that demonstrates functionality across the entire millimeter wave spectrum. A shallow rib waveguide supports a single transverse electric (TE) optical mode, and a Au coplanar waveguide (CPW) supports the modulating radio frequency (RF) mode.**

Keywords—$LiNbO_3$, modulators, photonics, thin-film

I. Introduction

With 5G wireless communications spanning into the millimeter wave region of the electromagnetic spectrum, RF systems are being challenged to span broader bandwidths. While such systems can consist of multiple, banded, subsystems, this comes at the expense of increased size, weight, and power requirements. An ideal solution would be to have a single system that accommodates such wide operational bandwidths in an economical as well as energy and spectrally efficient way. For this reason, this paper will introduce an RF-photonic system frontend that operates over ultra-broad bandwidths and can accommodate the emerging 5G spectral ranges. In particular, the enabling photonic device is a wideband electro-optic (EO) modulator that is used to up-convert RF signals directly at the RF front-end of a system. In so doing, the received RF signal becomes a sideband on an optical carrier that can be subsequently processed using simple optical lens. This technique has been shown to provide extreme RF signal fidelity, unlimited beam-bandwidth product (BBP), and the ability to implement multi-user MIMO.

The key to the up-conversion process is in the careful design of a wide bandwidth EO modulator. Herein we present the development of a crystal-ion-sliced (CIS) $LiNbO_3$ modulator that is suitable for commercial manufacturing. The substrate consists of a 700 nm thick *x*-cut $LiNbO_3$ device layer, affixed to a 500 µm thick quartz handle wafer via a 2 µm thick PECVD SiO_2 intermediate bonding layer. Shallow rib waveguides are formed by reactive ion etching (RIE) are utilized for guiding a single transverse electric (TE) optical mode, which are immediately adjacent to electroplated Au coplanar waveguides (CPWs) that support the modulating RF mode.

II. Device Design and Fabrication

Fig. 1 shows a single broadband CIS $LiNbO_3$ modulator fabricated in commercially available thin film $LiNbO_3$ on insulator procured from NanoLN. Utilizing a unique substrate such as this offers many benefits. RF substrate modes are able to be completely suppressed [1]. The index contrast in the optical waveguide is increased from a Δn of .001 to a Δn of ~0.5, permitting bent waveguides, and also reducing the optical mode size [2]. The optical mode size in a bulk device is normally ~8 µm in diameter; where the reduced optical mode size of our device is roughly 2 µm in diameter. The more concentrated optical mode allows for shrinkage of the gap between the electrodes. We see that shrinkage of the gap directly results in a DC V_π-L that is less than one fourth of what has been seen in similar broadband devices fabricated in bulk $LiNbO_3$ [3]. Neither pro nor con; using sub micrometer thick $LiNbO_3$ on quartz also affects the way we must approach index matching [4]. Index matching between the RF and optical modes in traveling wave devices has been addressed in bulk devices [3] and mechanically thinned devices [5], but not as

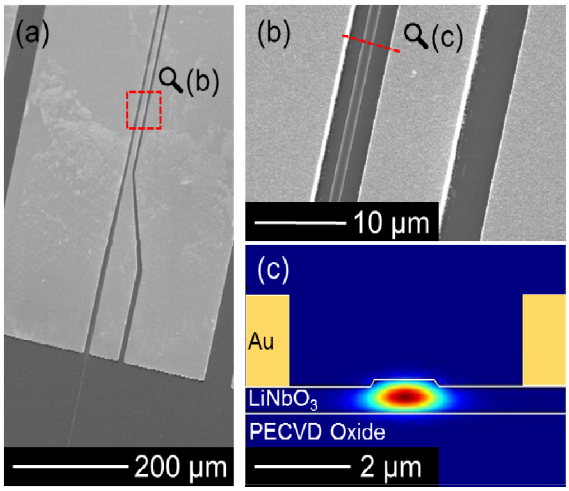

Fig. 1. Scanning electron microscope image of a fabricated device without the UV15 cladding layer. (a) Close up image of the unclad interaction region of the device. (b) Modal simulation of a guided TE optical mode in the device's cross section (c).

thoroughly for CIS devices [6]. If the indices are not adequately matched then the broadband functionality can be severely limited[4], [7].

A. Optical Waveguide

The effective optical index (n_{opt}) of the device is established by the physical properties of the optical waveguide. The rib in question is ~1.1 μm wide at the top and ~1.8 μm wide at its base; the etch depth is 160 nm. Lumerical FDTD Mode Solver is used to simulate the waveguide structure and provides an effective optical group index of 2.2608 for the fundamental TE mode, seen in Fig. 1(c). To form the optical waveguide an 80 nm thick chromium blanket layer is first sputtered onto the substrate. A softmask is patterned on top of the Cr layer with NR9-1500P photoresist from Futurrex. The softmask pattern is transferred into the Cr hardmask with a time multiplexed Cl based inductively coupled plasma (ICP) dry etch. After pattern transfer, any residual resist is removed in an O_2 plasma etch. The initial pattern is finally transferred into the $LiNbO_3$ with a directional, highly anisotropic lithium niobate etch, obtained using an ICP CF_4(6 sccm)/N_2(28 sccm)/O_2(0.5 sccm) etch. The etch is time multiplexed to prevent overheating of the sample. The number of cycles determines etch depth and each cycle consists of 1 minute etching in a 600 W plasma under 400 W bias. The etch rate of *x*-cut $LiNbO_3$ is ~27 nm per minute and the selectivity between $LiNbO_3$ and Cr is ~5.4:1. Any remaining Cr is stripped in a chemically selective wet etch, electrode deposition follows.

B. RF Waveguide

Electrodes in a coplanar ground signal ground configuration are built up directly on top of the CIS $LiNbO_3$ device layer using a gold electroplating process. The optical waveguide is situated in the gap between the signal and one of the ground pads. Design of these electrodes requires consideration most importantly of the effective RF phase index (n_{RF}) if broadband operation is required. The RF phase index must be matched with the optical group index and traditionally this is difficult to accomplish in bulk $LiNbO_3$ modulators as the RF index of lithium niobate is significantly higher than its optical index. However, in our hybrid material substrate, low dielectric constant quartz (ε_r = 3.8) [8] makes up the majority of this device. To this end matching indices calls for an increase in n_{RF}. With these factors in mind, by HFSS simulation, we are able to arrive at electrode dimensions in the modulator's interaction region for the thickness, signal width, and gap, of 1.8 μm, 9.5 μm, and 5 μm, respectively. The length of the fabricated interaction region is 0.92 cm. Of less significance than index matching, is the design of the input/output CPW launch region. A 150 μm long launch tapers into the interaction region over another 150 μm length. This launch design permits efficient coupling of the device to a standard 50 Ω transmission line and also makes it easier to probe or wire-bond to the device. The launch region in our design has a signal width of 53 μm, a gap of 10 μm, and a simulated broadband impedance of ~40 Ω.

C. Index Matching

Simulated n_{RF} values are extracted from HFSS models of the aforementioned device. At 110 GHz the simulated n_{RF} is equal to 2.02. The disparity between simulated n_{RF} and n_{opt} is ~0.24 and if fabricated, this device will have a reduced operational bandwidth. To achieve broadband operation the effective RF index requires further elevation. In other travelling wave devices, a proven method for increasing n_{RF} is cladding the modulator's interaction region in a higher index material, preferably a material with low RF loss and which is easy to apply, such as UV15 adhesive, possessing an RF index near 1.97 [9]. By adding a UV15 cladding layer to the HFSS model, the simulated n_{RF} at 110 GHz increases from 2.02 to ~2.26. The effect on the simulated optical group index according to modal simulations is a decrease from 2.261 to 2.244 which also helps to match modal indices overall. The simulated impedance of the air-clad interaction region is ~35 Ω up to 300 GHz; after application of UV15, this value drops to ~30 Ω.

Fabrication of the electrodes seen in Figs. 1(a) and 1(b) is accomplished in 4 major steps: seed layer deposition, photolithography, electroplating, and seed layer stripping. First a Ti:Au:Ti seed layer is deposited via electron beam evaporation; thickness of each individual layer is 100 nm resulting in 300 nm total thickness. Next, photolithographic definition of the electrodes is done with NR9-3000P photoresist from Futurrex. After photoresist development, the resist is hard-baked at 120 ℃ for 30 minutes to drive off excess solvent so that the resist is able to survive the final electroplating bath. Between lithography and electroplating, an O_2 plasma descum followed by a brief Ti wet etch in a hydrofluoric acid solution exposes the concealed Au seed layer. Au is then built up to the desired electrode thickness in an electroplating bath. Finally, photoresist and metal seed layers are stripped via iterated dips in H_2SO_4(3):H_2O_2(1) solution, deionized water, and KI based Au etchant. This cumulative process results in broadband CPW electrodes patterned directly on the $LiNbO_3$ surface. The previously simulated UV15 tuning layer is applied via brush to the device's interaction region, its thickness is roughly 20 μm. Flood exposure from a UV light source at a wavelength of 365 nm sets the epoxy in place. As a final step, single mode, polarization maintaining fiber V-grooves are aligned and bonded to the end facets of the device with UV curable Norland Optical Adhesive 61. Fiber V-groove bonding is not ideal but is required for high frequency testing on our RF probe station.

III. Characterization

Optical waveguide propagation loss of ~7 dB/cm is measured via cutback method. This result is comparable to propagation losses seen elsewhere in literature for dry etched ridge waveguides [2]. Although, through refined processing techniques similar devices reportedly demonstrate propagation loss as low as 0.4 dB/cm [10]. The total optical loss of the characterized 1.5 cm long modulator is ~40 dB; 10.5 dB of which can be attributed to the propagation loss. Remaining insertion loss is accounted for by the modal mismatch between single-mode optical fibers and $LiNbO_3$ waveguides. The spot size of the fibers possesses a Gaussian profile with an 8 μm

This work is sponsored by the U.S. Air Force Research Laboratory and the Air Force Office of Scientific Research.

waist and the asymmetric spot size of the rib waveguide according to modal simulation is ~2 µm laterally by ~0.7 µm vertically.

DC-V_π, scattering parameters, and optical sideband measurements are used to characterize this device. A DC-V_π of 3.4 V is measured by means of polarization rotation method[11], [12]. Fig. 2 shows two port scattering parameters are collected up to 110 GHz using an Agilent E8316C Programmable Network Analyzer (PNA), in conjunction with two Agilent N5260 T/R modules, and two 1 mm cable fed GGB industries probes featuring a GSG configuration with a 100 µm pitch. The same PNA setup is used to apply the modulating RF signal up to 110 GHz. An Agilent E4418-B power meter measures the RF power in this range. Above 110 GHz the measurements are conducted in three different frequency ranges, 110-170 GHz, 170-220 GHz, and 220-305 GHz. Each bandwidth corresponds with a PNA range extension module from OML, Inc., Millitech rectangular waveguides, and GGB Industries probes. Above 110 GHz an Erickson PM4 power meter captures the RF power before it enters the probe input. The device's optical output is fed directly into a Yokogawa AQ6319 Optical Spectrum Analyzer (OSA) and sidebands can be observed [13].

The resulting modulating spectrum was observed at the optical output, as shown in Fig. 3. CPW transmission lines were not terminated for the measurement. Optical sidebands up to 305 GHz are observed with a 6 GHz spacing between each measurement. Only upper sidebands are shown for clarity but each set of sidebands corresponds to the modulator's optical response normalized to the measured RF input power at the corresponding RF frequency. Probe insertion loss, feed loss, and harmonic generation in the RF source are all accounted for in the optical sideband normalization. Data for probe loss is supplied by the probe manufacturer. Feed loss is measured with the RF power meter. Harmonic generation is accounted for by observing unwanted sidebands for each measurement and adjusting the power table accordingly. Beyond 170 GHz a reduced power output from the sources inhibits our ability to account for harmonic generation and measurements become noisier as a result. The index matched modulator shows a frequency response up to the measured 305 GHz with a roll off of ~11 dB.

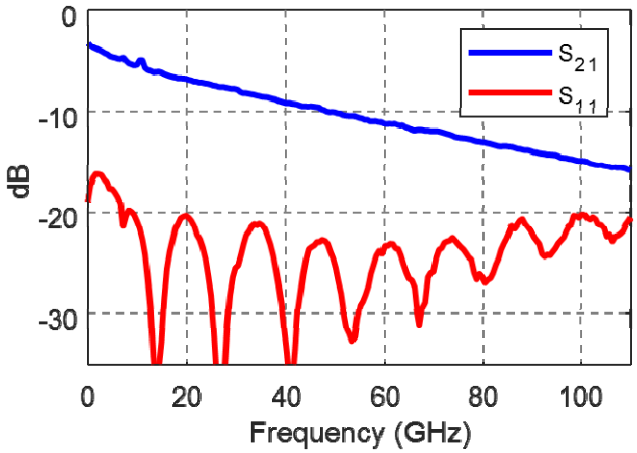

Fig. 2. Measured transmission S_{21} and reflection S_{11} parameters of a fabricated device's CPW electrodes.

IV. Conclusion

Presented in this paper is, to the best of our knowledge, the first instance of an index-matched travelling wave CIS $LiNbO_3$ modulator having a measured frequency response beyond 300 GHz. An interaction region cladding procedure is implemented to raise the RF effective index to match that of the optical effective index, yielding broadband performance. The combination of the modulator's excellent electro-optic performance and the flexibility of CIS $LiNbO_3$'s optical device design make it an ideal candidate for hybrid integration. The reduced mode size lends itself to poor coupling to single mode fiber; however, mode-matched coupling to and from other photonic devices and waveguides is an option[14]. Future work will require investigation of methods for efficiently coupling light into and out of the device, whether it be for hybrid integration or standalone use. Potential areas of continued research include incorporating broadband $LiNbO_3$ devices into hybrid photonic platforms such as Si or Si_3N_4 through the use of evanescent coupling [15]–[20], end-fire coupling [14], or structures such as grating couplers [21].

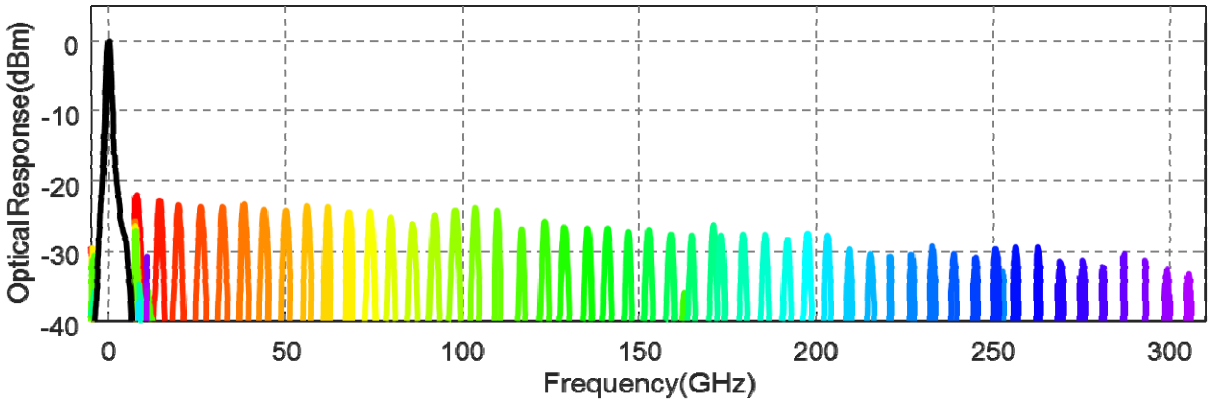

Fig. 3. Normalized optical modulation spectra of a 1550 nm optical carrier modulated up to 305 GHz. The spectra are symmetric but for clarity only the upper portion is displayed. Each sideband is normalized as if 0 dBm of RF input power were applied to the device electrodes. The device that produced these spectra has undergone the interaction region cladding procedure for index matching.

ACKNOWLEDGMENT

The authors gratefully acknowledge the support of Dr. Robert Nelson, and Dr. Attila Szep from the U.S. Air Force Research Laboratory as well as Dr. Gernot Pomrenke from the Air Force Office of Scientific Research, among other U.S. Government agencies.

REFERENCES

[1] Yongqiang Shi, "Micromachined wide-band lithium-niobate electrooptic Modulators," *IEEE Transactions on Microwave Theory and Techniques*, vol. 54, no. 2, pp. 810–815, Feb. 2006.

[2] G. Poberaj, H. Hu, W. Sohler, and P. Günter, "Lithium niobate on insulator (LNOI) for micro-photonic devices," *Laser & Photonics Reviews*, vol. 6, no. 4, pp. 488–503, Jul. 2012.

[3] J. Macario *et al.*, "Full spectrum millimeter-wave modulation," *Optics express*, vol. 20, no. 21, pp. 23623–23629, 2012.

[4] K. Aoki, J. Kondou, O. Mitomi, and M. Minakata, "Velocity-matching conditions for ultrahigh-speed optical LiNbO3 modulators with traveling-wave electrode," *Japanese journal of applied physics*, vol. 45, no. 11R, p. 8696, 2006.

[5] A. J. Mercante, P. Yao, S. Shi, G. Schneider, J. Murakowski, and D. W. Prather, "110 GHz CMOS compatible thin film LiNbO3 modulator on silicon," *Optics Express*, vol. 24, no. 14, p. 15590, Jul. 2016.

[6] V. Stenger *et al.*, "Engineered thin film lithium niobate substrate for high gain-bandwidth electro-optic modulators," in *CLEO: Science and Innovations*, 2013, p. CW3O–3.

[7] R. Spickermann, S. R. Sakamoto, and N. Dagli, "In traveling wave modulators which velocity to match?," in *Lasers and Electro-Optics Society Annual Meeting, 1996. LEOS 96., IEEE*, 1996, vol. 2, pp. 97–98.

[8] D. K. GHODGAONKAR, V. V. VARADAN, and V. K. VARADAN, "A Free-Space Method for Measurement of Dielectric Constants and Loss Tangents at Microwave Frequencies," p. 5.

[9] D. L. K. Eng, Z. Aranda, B. C. Olbricht, S. Shi, and D. W. Prather, "Heterogeneous Packaging of Organic Electro-Optic Modulators With RF Substrates," *IEEE Photonics Technology Letters*, vol. 28, no. 6, pp. 613–616, Mar. 2016.

[10] I. Krasnokutska, J.-L. J. Tambasco, X. Li, and A. Peruzzo, "Ultra-low loss photonic circuits in Lithium Niobate On Insulator," *arXiv preprint arXiv:1708.06787*, 2017.

[11] A. J. Mercante, D. L. K. Eng, M. Konkol, P. Yao, S. Shi, and D. W. Prather, "Thin LiNbO_3 on insulator electro-optic modulator," *Optics Letters*, vol. 41, no. 5, p. 867, Mar. 2016.

[12] D. L. K. Eng *et al.*, "Simple Fabrication and Processing of an All-Polymer Electrooptic Modulator," *IEEE Journal of Selected Topics in Quantum Electronics*, vol. 19, no. 6, pp. 190–195, Nov. 2013.

[13] Yongqiang Shi, Lianshan Yan, and A. E. Willner, "High-speed electrooptic modulator characterization using optical spectrum analysis," *Journal of Lightwave Technology*, vol. 21, no. 10, pp. 2358–2367, Oct. 2003.

[14] D. W. Grund, G. J. Schneider, J. Murakowski, and D. W. Prather, "Packaging and design of a heterogeneous dual laser chip for a widely tunable spectrally pure optical RF source," *Optics Express*, vol. 22, no. 17, p. 19838, Aug. 2014.

[15] L. Chen, M. G. Wood, and R. M. Reano, "125 pm/V hybrid silicon and lithium niobate optical microring resonator with integrated electrodes," *Optics Express*, vol. 21, no. 22, p. 27003, Nov. 2013.

[16] L. Chen, Q. Xu, M. G. Wood, and R. M. Reano, "Hybrid silicon and lithium niobate electro-optical ring modulator," *Optica*, vol. 1, no. 2, p. 112, Aug. 2014.

[17] L. Chen, J. Chen, J. Nagy, and R. M. Reano, "Highly linear ring modulator from hybrid silicon and lithium niobate," *Optics Express*, vol. 23, no. 10, p. 13255, May 2015.

[18] A. Rao *et al.*, "High-performance and linear thin-film lithium niobate Mach–Zehnder modulators on silicon up to 50 GHz," *Optics Letters*, vol. 41, no. 24, p. 5700, Dec. 2016.

[19] L. Chang *et al.*, "Heterogeneous integration of lithium niobate and silicon nitride waveguides for wafer-scale photonic integrated circuits on silicon," *Optics Letters*, vol. 42, no. 4, p. 803, Feb. 2017.

[20] P. O. Weigel *et al.*, "Lightwave Circuits in Lithium Niobate through Hybrid Waveguides with Silicon Photonics," *Scientific Reports*, vol. 6, p. 22301, Mar. 2016.

[21] M. Mahmoud, S. Ghosh, and G. Piazza, "Lithium Niobate on Insulator (LNOI) Grating Couplers," in *CLEO: Science and Innovations*, 2015, p. SW4I–7.